THE CONTRIBUTION OF INELASTICALLY SCATTERED ELECTRONS
TO HIGH RESOLUTION [110] IMAGES OF AlAs/GaAs HETEROSTRUCTURES

C.B. BOOTHROYD and W.M. STOBBS

Department of Materials Science and Metallurgy, University of Cambridge, Pembroke Street, Cambridge CB2 3QZ, UK

The effect of inelastic scattering on high resolution [110] images of GaAs/AlAs is analysed by comparing experimental and simulated images, with and without a centre-stop aperture. Inelastic scattering from the specimen alone is found to be insufficient to account either for the lack of compositionally dependent contrast or for the low visibility of the half spacings in the experimental images. It is shown using energy loss spectroscopy that surface contamination and ion beam damage layers contribute a sufficient proportion of both elastic and inelastically scattered electrons to centre-stop images that the associated weakly defocus-dependent lattice resolution detail can account for the overall form of the experimental images seen.

1. Introduction

The full characterization of AlGaAs/GaAs heterostructures requires the use of a mélange of "low" and "high" resolution electron microscopical techniques [1–5] some of which can be applied with confidence and ease while others need a great deal of care if they are to yield usefully quantitative information. The Al content of the layers can, for example, be obtained fairly easily either from the thickness fringe analysis of a cleaved wedge [6,7] (provided care is taken with the effects of absorption [8]) or from the 002 * dark field intensities of the respective layers [3], where in this case the use of a ratio technique allows surprisingly high accuracies [9]. The extent of any compositional intermixing at the interfaces can be deduced by the analysis of the Fresnel fringes produced in a through-focal series [10] given a knowledge now of the projected vicinality [11]. While this last technique can provide useful high resolution information indirectly, it is when we turn to the more

direct high resolution approach, as is necessary for the assessment of the interface roughness, that real difficulties arise. As the resolution required approaches the atomic level, the differential scattering of the respective layers out of the larger objective aperture needed is reduced. This is because substitution of aluminium for gallium causes only small changes in the average atomic scattering behaviour of the crystal, so that the mean intensities of layers of AlGaAs and GaAs are generally rather similar. Thus methods have to be found to enhance their relative visibility. Examining the interface with the electron beam in the [100] direction allows the composition-sensitive 002 and 020 reflections to contribute more than does 002 at [110] [12,13] thus enhancing layer contrast, but the direct observation of atomic steps is precluded at [100] if these lie, as expected, along ⟨110⟩ directions. As a more general solution we have thus suggested using a centre-stop aperture to exclude the 000 beam from contributing to high resolution images, so as to increase the relative contribution of the more composition-sensitive beams [14], and have analysed the technique for $Al_{0.3}Ga_{0.7}As/$ GaAs multilayers imaged along [100] [15]. While conventional image simulations suggested that there should have been an increase in the layer visibility, it was actually found that the layer

---

* Here, as in our previous paper [15], we take the layer normal to be (001) and differentiate, as before, between the way layers can be distinguished through differences in their overall *intensity*, the *contrast* of the atomic level detail or the *form* of the interference detail.

contrast was *reduced* and 0.28 nm lattice fringes tended to be much more apparent than the 0.14 nm fringes expected from $002/00\bar{2}$ interference, unless a low convergence was used. It was demonstrated that the 0.28 nm fringes originated in contributions to the image from electrons which had lost energy through plasmon scattering and had been scattered through angles large enough that a hollow cone of the 000 beam could pass around the centre-stop aperture [15]. It has actually also been shown that inelastically scattered electrons contribute significantly to 002 dark field images, as used for measurements of the Al content of the layers [9], as well as to the Fresnel fringe images used for measurements of the interface diffuseness [16].

In the light of increasing evidence that electrons which have undergone inelastic losses can contribute significant atomic-level detail in high resolution images (e.g., refs. [5,17,18]) we have continued our previous work, noted above, on the use of centre-stop images for the examination of AlAs/GaAs multilayers imaged along the [100] direction [15]. In this paper we concentrate on the behaviour of the images formed with the beam in the [110] direction, which is more technologically interesting, and also attempt to make a more quantitative comparison of the simulated and experimental images obtained in order to determine the relative importance of the variety of types of contribution to such images.

After describing briefly the image simulation techniques we have used (section 2, given in more detail in our previous paper [15]), we go on to discuss the characteristics to be expected for conventional and centre-stop images of AlAs/GaAs interfaces at [110] in section 3. While there are interesting differences in, for example, the effects of specimen tilt on such simulations as seen around [100] [15], we provide only a limited description of even the centre-stop simulations since these bear little relation to the otherwise excellent experimental images which can be obtained (section 4). In searching for the reasons for this discrepancy (discussed in section 5) we have made an analysis, using electron energy loss spectroscopy (EELS), of the relative magnitudes of the elastic and inelastic contributions which must be made to an image

and give the results of this investigation in section 6. We conclude (section 7) that the effects of specimen contamination, in effectively increasing the convergence onto the specimen, are much more important than for conventional images, particularly at low specimen thicknesses.

2. Simulation methods

Computer simulations were performed in a similar way to those reported earlier [15] in which the unit cell used was a 6×1 periodically continued supercell of three AlAs and three GaAs unit cells sampled in a 256×32 point array. Inelastically scattered electrons are focussed by the objective lens to give a more overfocus image than is formed by the elastically scattered electrons, so the former contributions to the overall image were included in the simulations by the incoherent addition of images of different defoci weighted according to an energy loss profile. Thus the contributions from inelastically scattered electrons are taken to be the same as would be obtained from elastically scattered electrons of reduced energy at a higher (less negative) defocus that have traveled through the full specimen thickness. This might at first seem to be an oversimplification since classically an electron could suffer an inelastic scattering event at any stage of its travel through the specimen. However, for the predominant single electron and plasmon scattering events little phase information is lost during the inelastic scattering processes provided the scattering is through a small angle and essentially intraband [19]. On this basis, then, it does not matter whether the scattering occurs near the top or the bottom of the specimen. The effects of higher energy loss (≥ 20 eV) or higher angle (e.g. phonon) processes were neglected in the calculations. Phonon processes would not, in any case, be expected to produce high resolution *detail*, their main effect being to add a uniform background intensity to the images [17]. Since normal phenomenological methods of including "absorption" in multislice calculations are designed to model inelastic scattering as an addition of a constant background intensity, it was not considered relevant to include them here.

3. [110] Simulations

In order to understand the behaviour of the centre-stop simulations we must first consider briefly the form of bright field images at [110] of an AlAs/GaAs multilayer as a function of thickness and defocus, noting the relatively minor, though still "pattern changing", effects of incorporating contributions to the image detail due to inelastically scattered electrons. A set of such simulations incorporating the contrast from sub 20 eV loss electrons in exactly the same way as was done for the [100] beam direction [15] is shown in fig. 1b, including a comparison with a conventional elastic simulation for thickness of 48 nm (fig. 1a). These and all subsequent simulations were calculated for an objective aperture whose resolution limit was 0.18 nm. This provides a first approximation to the imaging behaviour of the Cambridge HREM at 500 kV, and the simulation
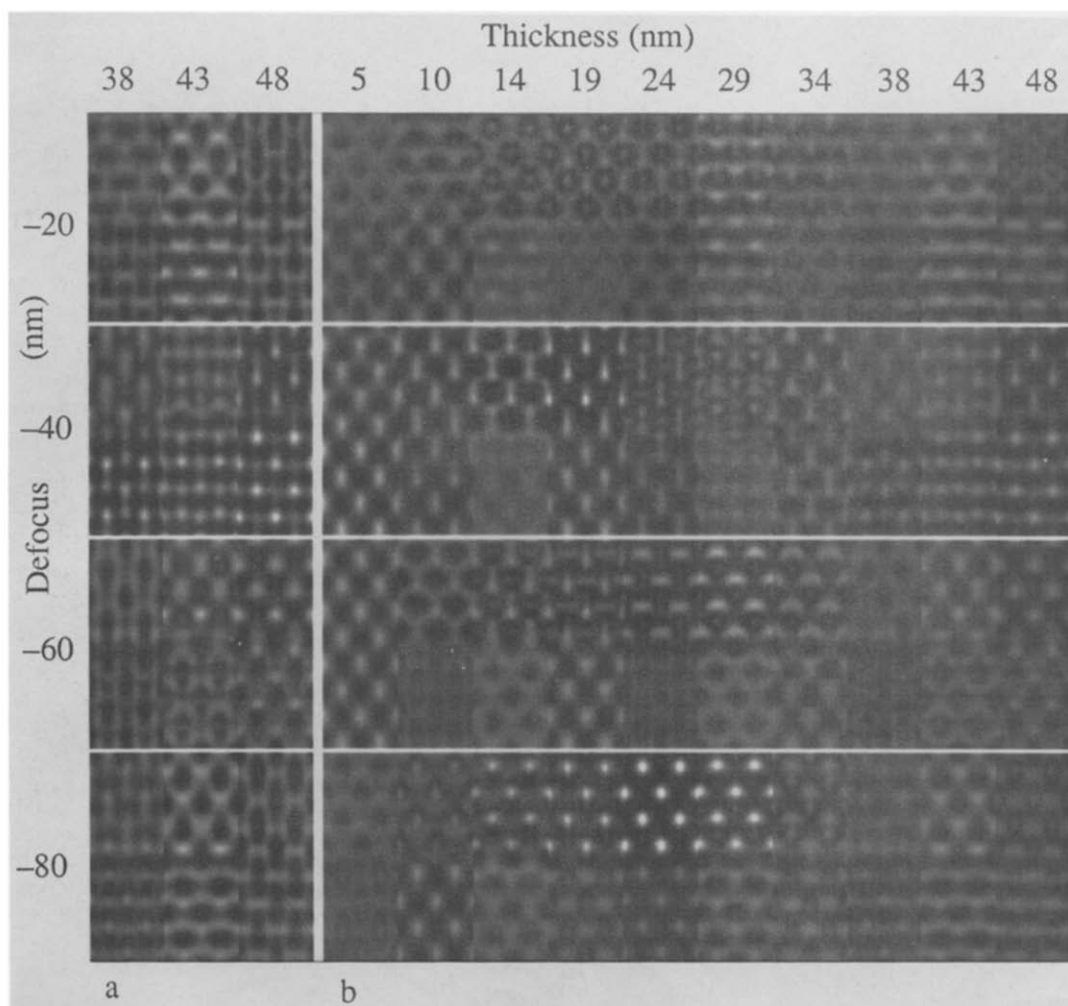

Fig. 1. Simulated images of an AlAs/GaAs interface (AlAs at the top) imaged with the beam parallel to [110], a resolution cut-off at 0.18 nm and assuming: (a) elastic scattering only and (b) with the contributions from plasmon scattering included. In these and all following image simulations each image is calculated with the same intensity scale relative to the incident electron beam intensity (=1) and is printed with zero electron intensity as black. The electron intensity corresponding to white in the figure (I_{white}) and the maximum intensity of the original image (I_{max}) are given for each figure. In this case, $I_{white} = 3$ and $I_{max} = 3.56$.

parameters used were appropriate for this instrument for which Scherzer defocus is at −62 nm. The full effects of convergence were not included by the incident beam tilt method, but this will not detract from the accuracies of the simulations at the level required. The image interference patterns are very sensitive to small changes in both thickness and defocus, as is well known for this normal (e.g., ref. [20]). The average intensities of the AlAs and GaAs layers are about the same (and indeed would both be equal to the incident intensity had the simulation been done without an objective

aperture) and the phase contrast from the 3.4 nm period multilayer (or equivalently the Fresnel contrast at the interface) is small, so that the layers are distinguished mainly by their differences in pattern, most pronounced at thicknesses between 14 and 29 nm where the 000 beam for GaAs is of higher intensity than that for AlAs which goes through a minimum in this thickness range. Outside this thickness range the layers look more similar and can be distinguished only by generally smaller differences in either the pattern or the contrast of the lattice fringes which would be
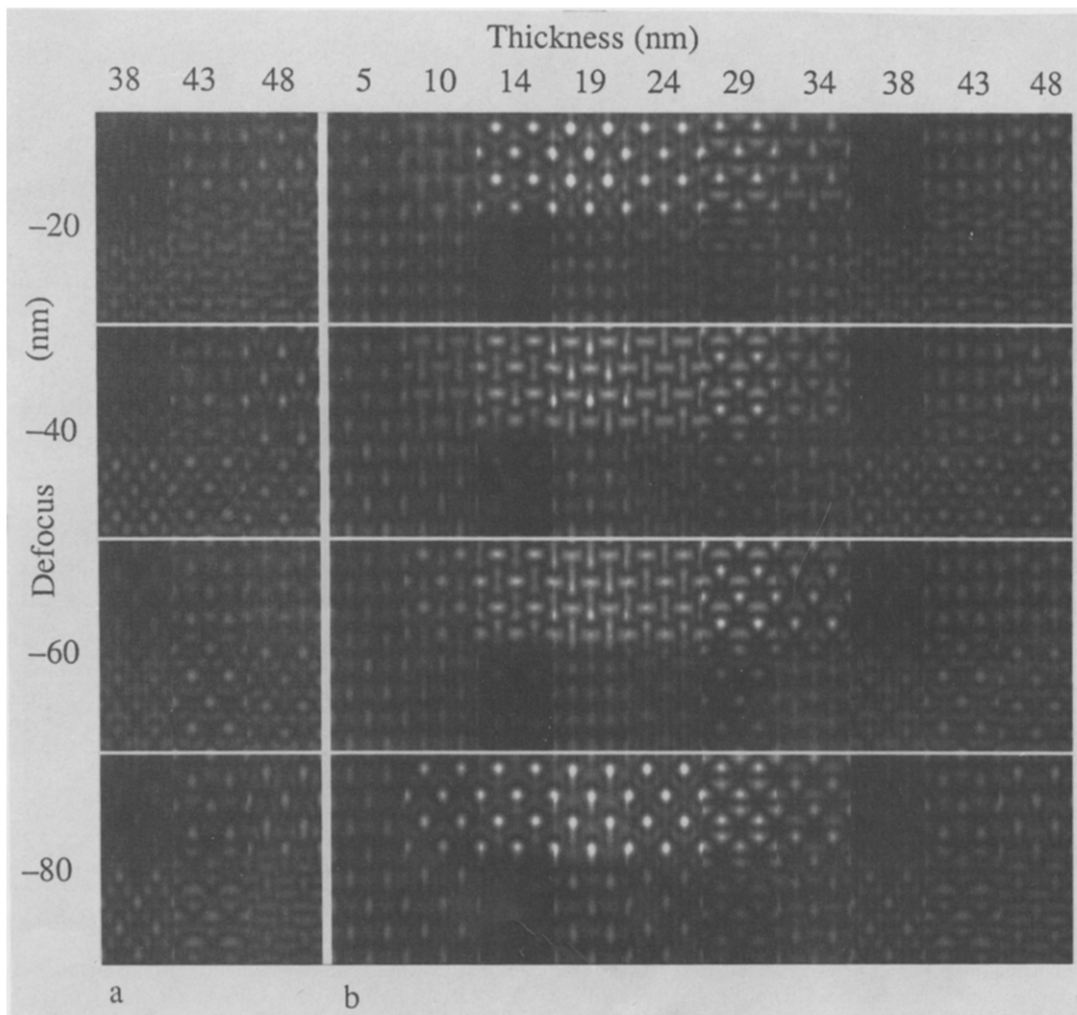

Fig. 2. Simulated images as for fig. 1 but with a centre-stop aperture whose inner cut-off corresponds to 0.6 nm: (a) is calculated assuming only elastically scattered electrons whilst (b) includes inelastically scattered electrons. $I_{white} = 1.5$ and $I_{max} = 2.22$.
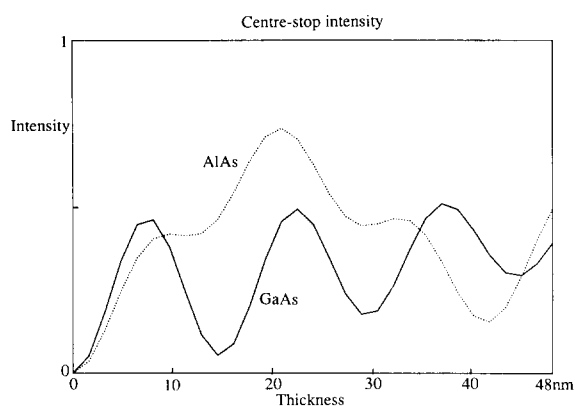
Fig. 3. Calculated average intensity of centre-stop images of GaAs (———) and AlAs (·····) as a function of thickness. These have been calculated by subtracting the intensity of the 000 beam from 1 (the intensity of a bright-field image with no objective aperture).

unlikely to be detectable experimentally. Thus the importance of including the effects of inelastic scattering, even for these conventional images, may be noted on comparing the changes in "pattern" with the inclusion of inelastic scattering for, for example, $\Delta f = -80$ nm and a thickness of 48 nm.

Fig. 2 shows images calculated under the same conditions as fig. 1 except that now a centre-stop aperture excludes the 000 beam. The AlAs and GaAs layers can now be distinguished much more easily than before through their large variations in average intensity as a function of thickness, particularly at thicknesses between 14 and 29 nm where the AlAs has a much greater intensity than the GaAs layer. The reason is demonstrated more clearly in fig. 3 where the average intensity for AlAs and GaAs in a centre-stop image is plotted as a function of thickness. Up to a thickness of about 14 nm the GaAs layer should be marginally brighter than the AlAs layer, while between 14 and 34 nm the AlAs layer is expected to be much brighter than that of GaAs. Above 34 nm the relative intensity of the layers oscillates more rapidly, and at lower contrast, so that the layers should then again be distinguished mainly through their pattern differences. It is the improvement in the visibility of the layers, by the increase in both contrast and the intensity differences across them

for such simulated centre-stop images, which has provided the main motivation for their analysis. However, it is also interesting that, at [110], the position of the interface is fairly clearly defined, in contrast to its appearance in similar simulations for a [100] beam direction, at least for lower Al content.

In our previous analysis of centre-stop images at [100] we found that it was important to include the image detail contributed by electrons which had undergone a loss and been scattered into a hollow cone around the centre-stop [15]. We show the effect of including such electrons for the [110] beam direction in fig. 4, the calculation being performed in the same way as previously with the same fairly arbitrary assumption that about half the electrons scattered inelastically could contribute in this manner. (In these and the other calculations described, the relative number of elastic and inelastic electrons was determined on the basis of the electron energy loss behaviour at 100 kV as noted in section 2.) Thus fig. 4a shows the images formed by the elastically scattered electrons plus the half of the loss electrons which are scattered through angles smaller than the radius of the centre-stop aperture for three thicknesses. Fig. 4b shows the images produced by the portion of the inelastically scattered electrons scattered through angles larger than the radius of the centre-stop for the same thickness, and the sum of these images is shown in fig. 4c for an extended range of thicknesses. At 14 nm thickness the layer contrast is high since the GaAs intensity is at a minimum (see fig. 3) while the 29 nm thickness corresponds to the second minimum in the GaAs intensity. From 34 to 38 nm in thickness the layer contrast is reversed, whilst above 38 nm there is little difference in the GaAs and AlAs average intensities. There is little difference in pattern between the simulations with (fig. 4c) and without (fig. 2b) the inelastic hollow cone contributions, but the overall contrast is reduced owing to the addition of relatively coarse detail at low intensity (note the changes of intensity scale between figs. 4a, 4c and 4b). The reason why in this case, at [110], inelastic scattering around the centre-stop appears to have less effect than at [100] is that the elastic contribution to the image from the {002} and {111}
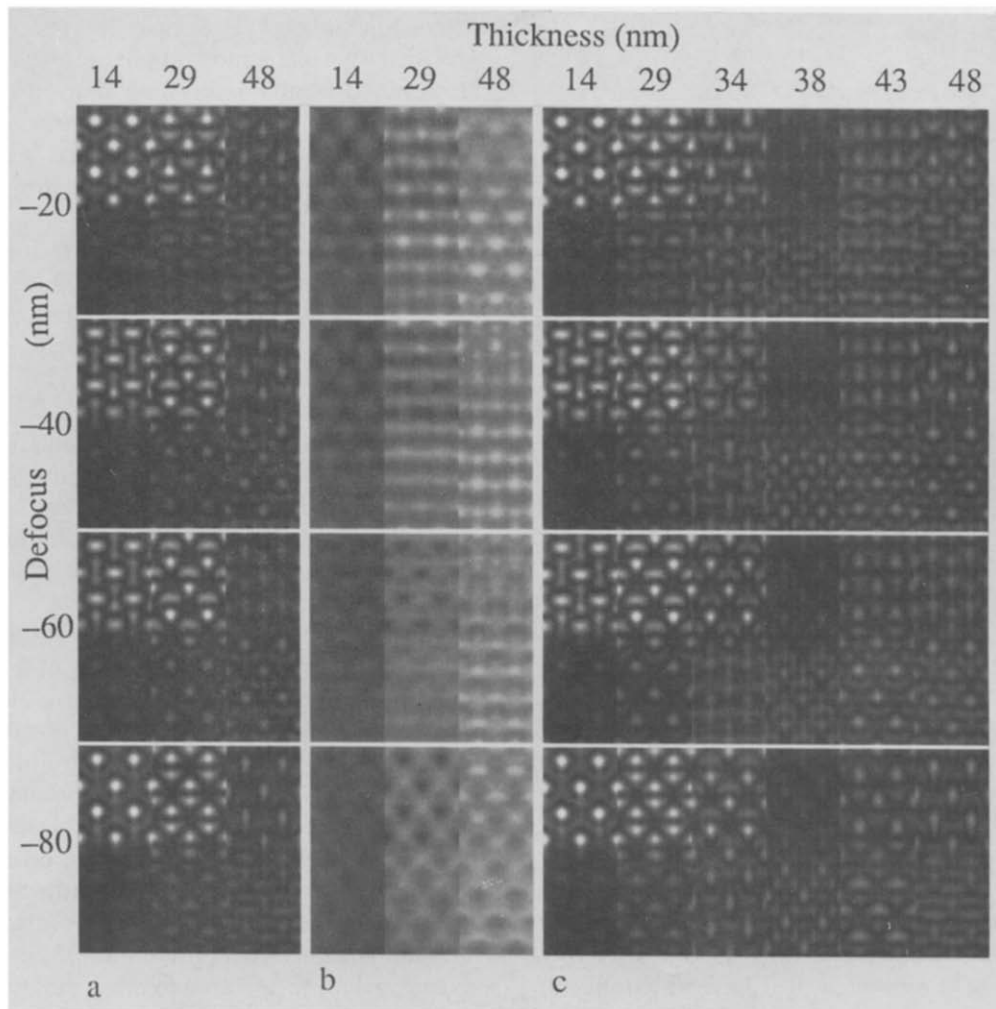
Fig. 4. Simulated images of an AlAs/GaAs interface imaged with a centre-stop aperture as for fig. 2. In (a) we include the elastically scattered electrons plus the half of the inelastically scattered electrons which are scattered through angles less than the radius of the centre-stop aperture and contribute dynamically through their further elastic scattering; (b) shows the contribution made by the remainder of the electrons which are scattered inelastically through angles greater than the centre-stop radius as a hollow-cone bright-field image and (c) is the sum of both contributions (a) and (b). For (a) $I_{white} = 1.5$ and $I_{max} = 2.11$, for (b) $I_{white} = 0.2$ and $I_{max} = \sim 0.25$, whilst for (c) $I_{white} = 1.5$ and $I_{max} = 2.13$.

beams is stronger than that due to the {002} and {220} beams for similar thicknesses. If the specimen is tilted away from [110] by a rotation about [1$\bar{1}$0], then the contribution from the {111} beams decreases dramatically. Centre-stop image simulations for AlAs/GaAs tilted by 6.1° away from [110] are shown in fig. 5a. Now, with the normal elastic contribution to the simulations of much lower intensity, the 0.28 nm fringes characteristic

of electrons scattered inelastically around the centre-stop are more visible in the GaAs layers. Similar images for an $Al_{0.3}Ga_{0.7}As/GaAs$ multilayer are shown in fig. 5b for a more direct comparison with our previous results for the [100] beam direction [15], and now the layers are almost indistinguishable with the 0.28 nm fringes evident in both the $Al_{0.3}Ga_{0.7}As$ and the GaAs layers.
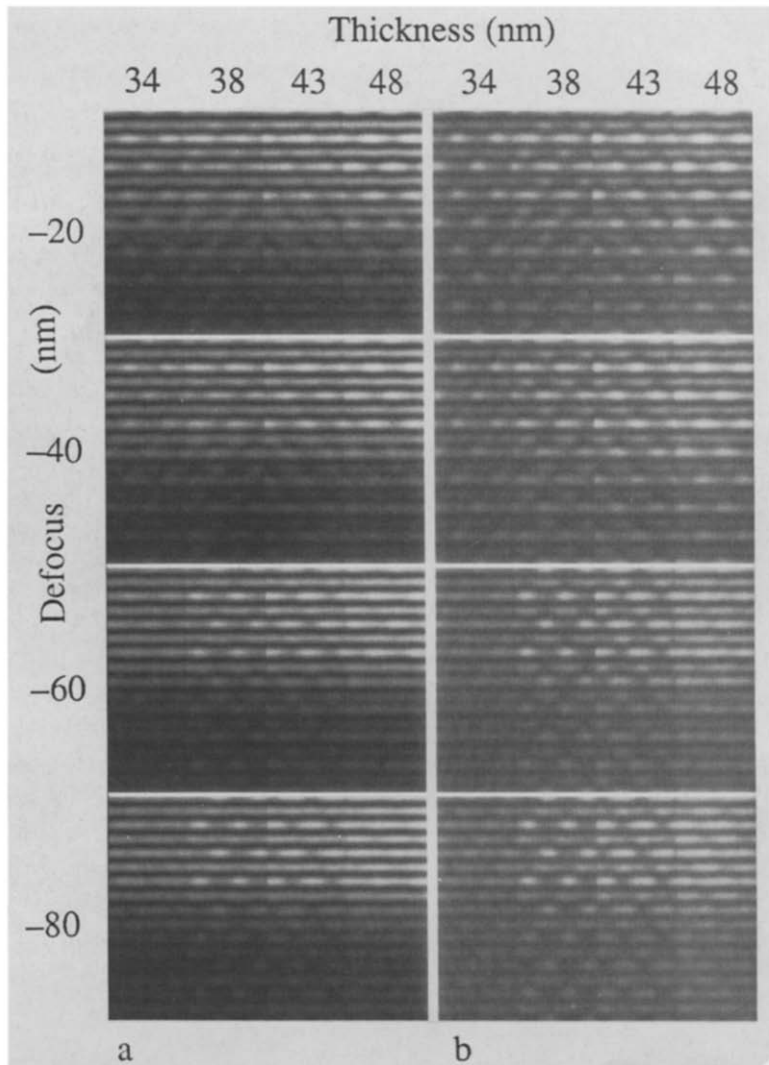
The interesting inference we can make from

Fig. 5. Simulated images as for fig. 4c including the effects of electrons scattered around the centre-stop aperture but now with the specimen tilted by 6.1° about the layer normal (001) for (a) an AlAs/GaAs interface and (b) an $Al_{0.3}Ga_{0/7}As$/GaAs interface. For (a) $I_{white} = 1.0$ and $I_{max} = 1.0$ whilest for (b) $I_{white} = 0.45$ and $I_{max} = 0.45$.

these simulations is that centre-stop images at [110] should be much less strongly affected by inelastically scattered electrons passing around the centre-stop than proved to be the case for otherwise similar images at [100]. This is because, by comparison, the contribution from electrons scattered around the centre-stop is roughly constant as a function of specimen tilt. However, as we shall see below, the experimentally obtained centre-stop images at [110] still show much less

layer contrast than is predicted on the basis of the simulations described above.

4. Experimental images at [110]

Fig. 6a shows a through focal series of bright field images of an AlAs/GaAs multilayer whose thickness increases (with some local variation) from left to right. Like all the images presented
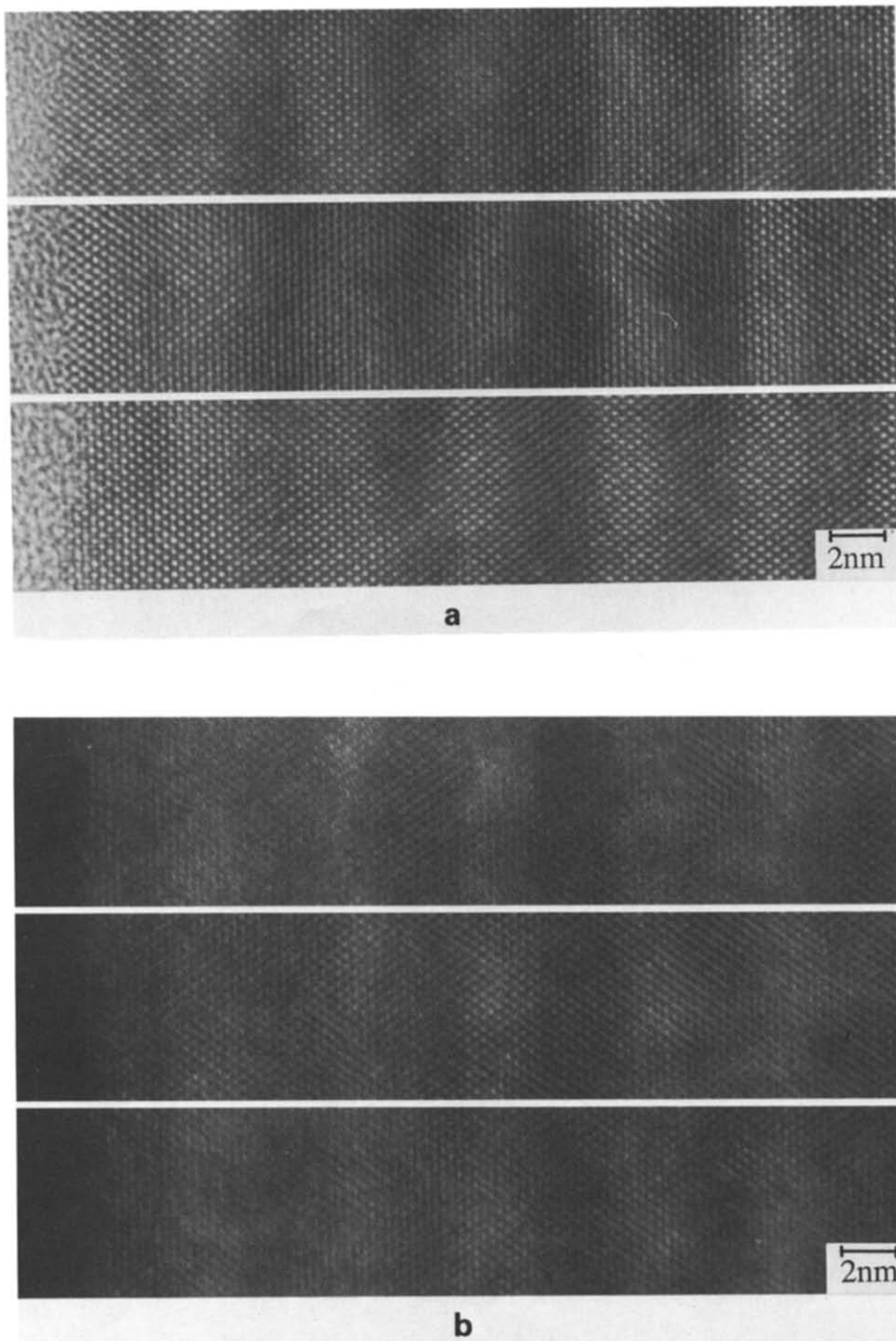
Fig. 6. Images of an AlAs/GaAs multilayer with the beam along [110] using (a) no aperture and (b) a centre-stop aperture. The defocus values for (a) are: top $\Delta f = -60$ nm, middle $\Delta f = -85$ nm and bottom $\Delta f = -110$ nm, for (b) the defocus change between each image was the same as (a) but it is not possible to determine the absolute values. For both (a) and (b) the thickness increases from left to right.

here, they were taken using the Cambridge University high resolution electron microscope operated at 500 kV. At all defoci the AlAs layers are brighter (i.e. they have a higher average intensity) than the GaAs layers, and this effect is maintained or even enhanced as the thickness is increased. In addition the lattice fringe contrast is highest within a few lattice fringes of the specimen edge and decreases as the thickness increases. Centre-stop images from the same area of the specimen are shown in fig. 6b from which it can be seen that again the AlAs layers are *always* brighter than the GaAs layers, and that there are very few of the half-spacing fringes predicted by the simulations in fig. 2, particularly near to the specimen edge where the best agreement between experimental and simulated images would be expected. Indeed the centre-stop images look very like the bright field images! Thus, while for the bright field images the high resolution detail is similar, at least qualitatively, to that predicted by the simulations (fig. 1), the centre-stop images exhibit less of the high frequency information than would be expected and the intensity distribution is totally dissimilar to that predicted, even allowing for the effect of hollow cone inelastic contributions.

A better idea of how the average image intensity changes with thickness is gained from fig. 7 where the average intensity is plotted as a function of thickness from densitometer traces across a
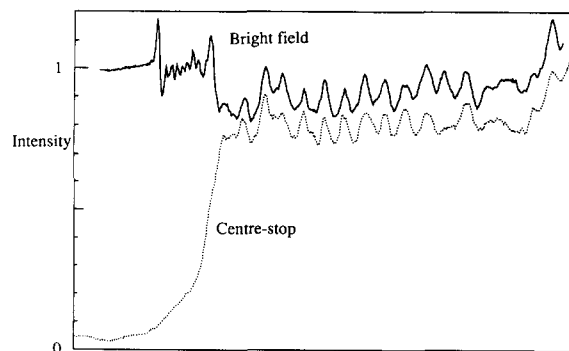

Fig. 7. Average intensity (i.e. ignoring lattice fringe detail) of a bright-field (——————) and a centre-stop (· · · · ·) image whose thicknesses increased towards the right from zero (no specimen) at the left. Both traces are plotted on the same scale where the incident intensity is 1 and in both cases the AlAs layers are brighter than the GaAs layers at all thicknesses.

bright field and a centre-stop image. For the bright field image the average intensity of the contamination layer is 1 (the incident intensity), but the AlAs layers have an intensity of about 0.95, while that for the GaAs layers is only about 0.85. This reduction in intensity is caused by the electrons that have been scattered outside the microscope objective lens and thus lost from the image. The proportion lost is dependent on atomic number, so that more electrons are lost from the GaAs layers than from the AlAs layers. The average intensity for the centre-stop image (fig. 7) is about 80% of the bright field intensity *both* for the GaAs *and* for the AlAs layers and, still more significantly, this high value seems to be relatively independent of specimen thickness. This is in contradiction to the average intensities for centre-stop images obtained for simulations on the basis that the scattering is purely elastic (as shown in fig. 3): the intensity of the GaAs layers should oscillate between 0 and about 0.5 whilst the AlAs layer intensity should rise from 0 to about 0.7 at a thickness of about 20 nm, then fall again to reach a minimum at ~ 45 nm. Thus the intensities of the experimental centre-stop images are higher than those predicted by the simulations and have none of the expected variations with thickness. A clue to the source of the extra intensity in the centre-stop images lies in the behaviour of the contamination layer. Its intensity rises to about 0.3 in the centre-stop profile (fig. 7) where the first GaAs layer begins, and thus if it is assumed that the contamination layer is of uniform thickness we would expect, to a first approximation, an intensity of 0.3 from the contamination layer to be added on to the entire centre-stop image.

Reduction of the incident beam convergence should reduce (but not eliminate) the contribution to the images from electrons which have undergone losses whilst leaving the contribution from the carbon layer virtually unchanged. Thus images taken with a lower convergence should exhibit more half-spacings than those taken with higher convergences in just the same manner as was found to be the case at [100] [15]. Fig. 8 shows two centre-stop images of the same area of an AlAs/GaAs multilayer tilted away from [110] and with a higher beam convergence for fig. 8a than
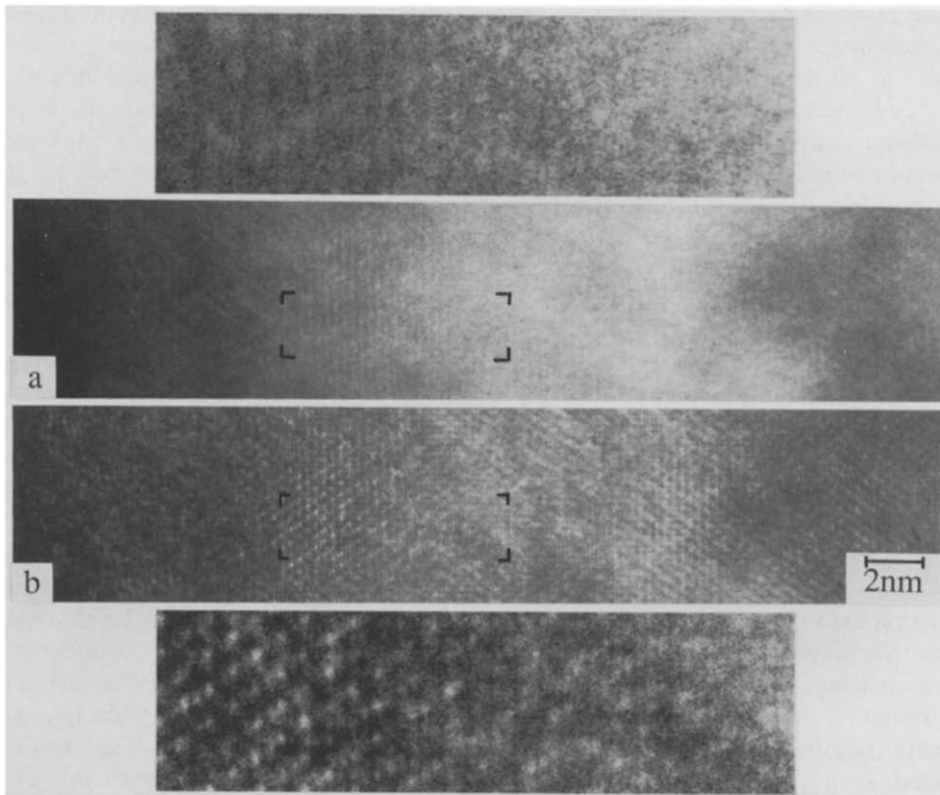
Fig. 8. Centre-stop images of the same area of an AlAs/GaAs multilayer tilted slightly away from [110] (a) with a high incident beam convergence and (b) with a much lower convergence. The centre portion of each image is enlarged to show the absence in (a) of the finer lattice spacings that are seen at the lower convergence for (b).

for fig. 8b. The half-spacings are indeed more predominant in fig. 8b than in fig. 8a but the overall intensities were again (as for fig. 7b), and even on a qualitative basis, anomalous.

5. Discussion of the centre-stop image intensity anomaly

Any discussion of the high resolution contrast of centre-stop images must take into account the source of all the electrons contributing to the image. We have seen that both the high resolution detail and the average intensities of the centre-stop images are in disagreement with simulations based on elastic scattering in that they are of too high an intensity and exhibit too few half-spacing fringes. It is thus likely that some of the extra intensity is

responsible for the larger spacing fringes. What then are the possible sources of the extra intensity?

The effect on the image intensity of inserting a centre-stop aperture is to prevent those electrons which hit the aperture from contributing to the image. This is equivalent to subtracting the intensity of a bright field image, formed using an ordinary objective aperture of diameter equal to the diameter of the centre-stop, from the average (i.e. excluding high resolution detail) intensity of an image obtained with no aperture. Hence the average intensities of the centre-stop image simulations of GaAs and AlAs plotted in fig. 3 were obtained by subtracting the 000 beam intensity from 1 (since we neglected here the effect of scattering differences outside the objective aperture). However, as can be seen from the intensity

trace (fig. 7) of the real images taken with no objective aperture, electrons are scattered beyond the acceptance angle of the objective lens more for the GaAs than for the AlAs. Thus a better estimate (provided we knew the specimen thickness) of what the centre-stop profile of fig. 3 should look like would emerge from subtracting the calculated 000 beam intensity from the bright field trace of fig. 7. Since in fig. 7 the AlAs layers are always brighter than the GaAs layers in the bright field trace, the effect on fig. 3 would be to decrease the intensity of the GaAs more than that of the AlAs, thus making the layering more visible at most thicknesses and reversing the layer contrast at low thicknesses so that the AlAs layers would become brighter than the GaAs layers here too. While this latter effect is seen experimentally, the effect of scattering outside the objective aperture overall should be to *increase* the layer *contrast* in the centre-stop images, whereas, experimentally (fig. 7) the contrast observed is almost the same as that of the bright field image and *lower* than predicted.

The effects of contamination on the signal-to-noise ratio of high resolution images have been considered by Gibson et al. [21] who showed that for argon-ion-thinned silicon the noise level was about 8% of the incident beam intensity. However, although our images do contain a high level of noise, this cannot affect the average intensities measured here. It was noted in section 4 that the contamination layer (which also of course includes the beam-damaged surface of the specimen) has an intensity of about 0.3 at the edge of the GaAs. If it is assumed that this layer continues over both surfaces of the specimen, one might expect to a first approximation a uniform intensity of about 0.3 to be added to the centre-stop intensity at all specimen thicknesses. This is an oversimplification, in fact, since it is well known that, at least for conventional dark field images, it is possible to obtain images for which the contamination layer is brighter than the specimen. More accurately, the effect of an amorphous layer on the top surface of the specimen is to scatter electrons sideways both elastically and inelastically so that the beam incident on the GaAs has a higher convergence than it would otherwise have had and contains a signifi-

cant proportion of inelastically scattered electrons before it enters the GaAs.

It is thus qualitatively clear that the contamination layer on the specimen surface can scatter a significant number of electrons both elastically and inelastically to angles high enough to pass around the centre-stop aperture. Accordingly, in order to see whether or not such an effect can provide an explanation for the differences between the observed centre-stop images and the simulations, we now discuss the results of measurements made of the intensity distribution as a function of angle and energy loss for GaAs using electron energy loss spectroscopy (EELS).

6. Electron energy loss spectroscopy

The EELS measurements were made on a Philips 400ST operated at 100 kV equipped with a dual parallel/serial energy loss spectrometer [22] with the aim of measuring the elastic and inelastic intensities as a function of GaAs specimen thickness for images both with and without a centre-stop aperture. Since no centre-stop aperture was available for the 400ST microscope the centre-stop intensities were determined by subtracting the intensities obtained with a small conventional objective aperture from the intensities measured with no objective aperture. The intensities as a function of specimen thickness for the cases of no objective aperture, a small objective aperture and a centre-stop aperture are shown in fig. 9. EELS spectra were measured up to an energy loss of about 300 eV, and the total area of each spectrum is taken to represent all the scattering since the intensity scattered beyond 300 eV was negligible. The lines for "elastic" scattering include all the intensity in the zero loss peak up to the minimum between it and the first plasmon peak and thus include some single electron losses and phonon scattered electrons as well as the solely elastically scattered electrons. The lines for inelastic scattering were obtained by subtracting those for elastic scattering from the total scattering. For all graphs in fig. 9 the value plotted at zero thickness was obtained from a spectrum taken from the contamination layer adjacent to the thinnest part of the speci-
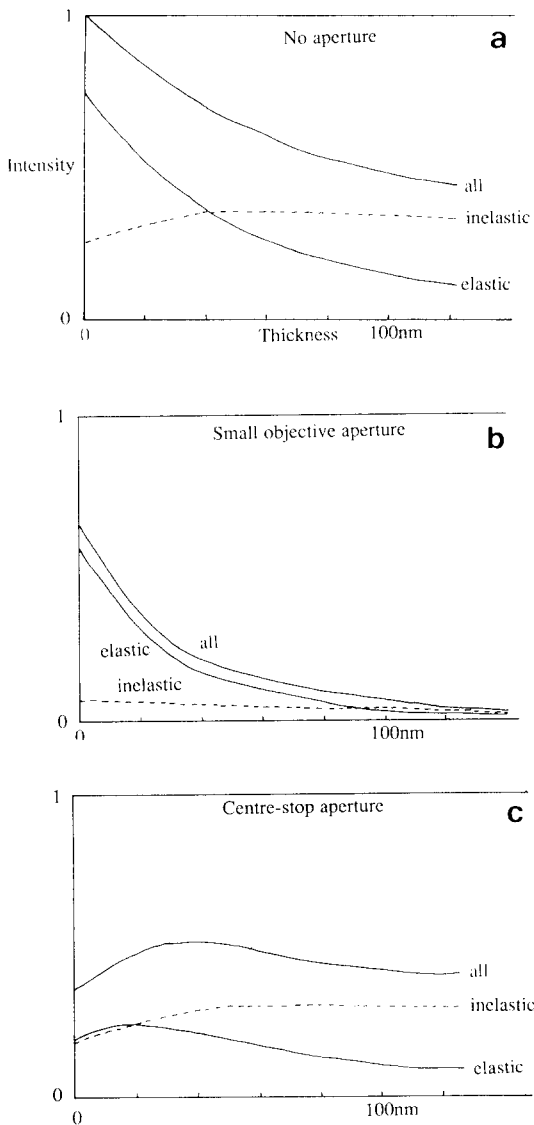
Fig. 9. Image intensities as a function of specimen thickness measured using EELS for (a) no objective aperture, (b) a small objective aperture and (c) a "centre-stop aperture", calculated by subtracting (b) from (a). The intensity at zero specimen thickness corresponds to the intensity of the contamination layer imediately adjacent to the specimen. The lines for "all" scattering represent the total area of the spectra taken and include losses up to 300 eV. The lines for "elastic" scattering include electrons in the zero loss peak up to the minimum (~ 8 eV) between it and the first plasmon peak, whilst the lines for "inelastic" scattering were obtained by subtracting the elastic scattering from the total scattering. For all graphs, an intensity of 1 represents the incident intensity.

men. Considering first the case where no objective aperture was present, fig. 9a shows that the con-tamination layer does not scatter electrons to suf-ficiently high angles that any are lost from the image, but about 25% have been inelastically scattered. At greater thicknesses the intensity of the inelastically scattered electrons increases only slowly to reach a maximum, at about 60 nm, of 0.35 but even so, above a thickness of 40 nm the proportion of inelastically scattered electrons is greater than that of the elastically scattered elec-trons. When a centre-stop aperture is present, as in fig. 9c, the contamination layer would contrib-ute an intensity of as much as 0.35 at zero "speci-men" thickness and roughly half of these electrons would have undergone inelastic losses. With in-creasing specimen thickness the proportion of in-elastically scattered electrons increases so that in a centre-stop image a minimum of half of the elec-trons contributing to the image have been scattered inelastically.

Unfortunately, it is not easy to relate these measurements made at 100 kV to the images taken at 500 kV. The total elastic and inelastic scattering cross sections both decrease with accelerating volt-age ($\sigma \propto \lambda^2$) [23] so that their ratio remains roughly constant, but in addition their angular distribu-tions change so that the ratio of elastic to inelastic scattering within an aperture of a given radius (or even a radius of a given fraction of a reciprocal lattice spacing) varies with accelerating voltage. However, general conclusions can be drawn by considering the results for low specimen thick-nesses at 100 kV since similar intensities are scattered by the contamination layer into the centre-stop image at 500 kV (0.35 for 100 kV and 0.3 for 500 kV). Given that the centre-stop image contains as much inelastic as elastic scattering, simulated images (fig. 10) were calculated as for fig. 4 (where plasmon scattering around the centre-stop was included) but now with an in-tensity of 0.3 subtracted from the beam that is undeviated and hits the centre-stop and a similar intensity added to the beams that are scattered round the centre-stop, of which 0.15 was taken to be scattered elastically and 0.15 scattered inelasti-cally (plasmon). This should provide a reasonable approximation, on the basis of the EELS data, for

Thickness (nm)

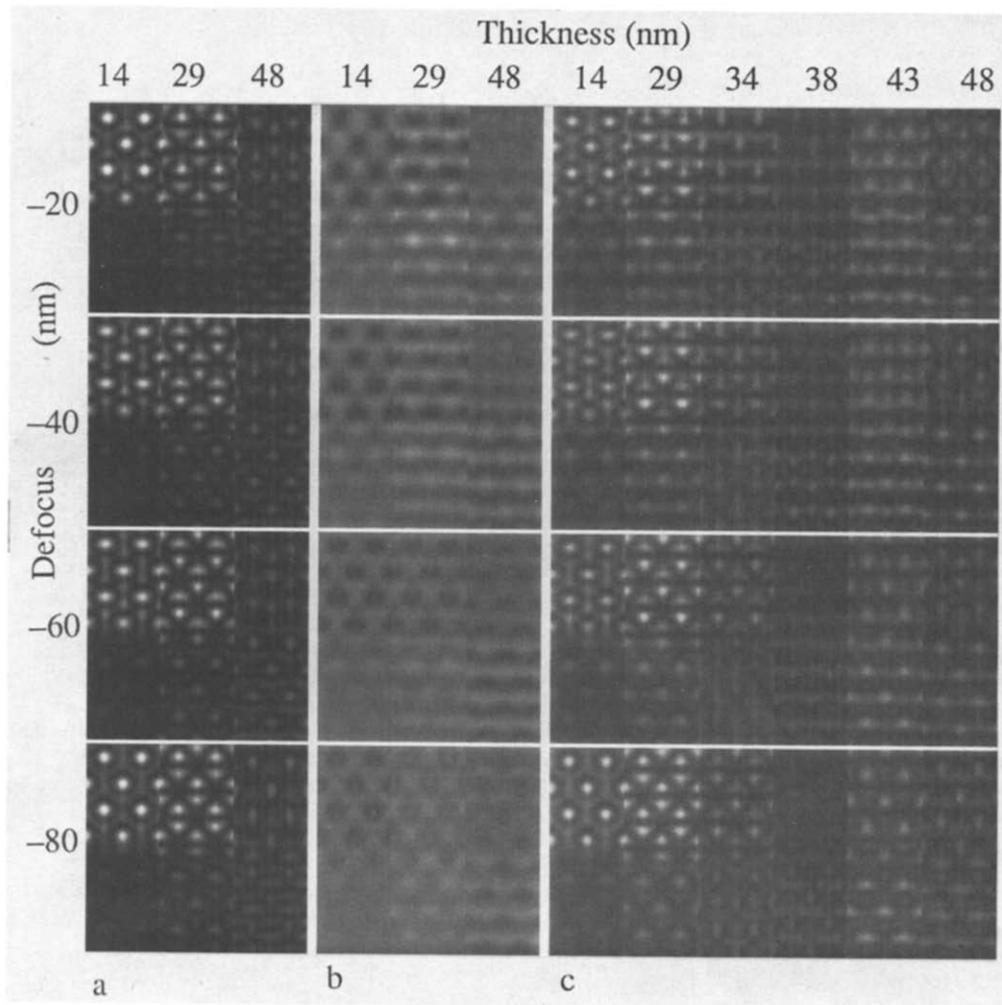| 14 | 29 | 48 | 14 | 29 | 48 | 14 | 29 | 34 | 38 | 43 | 48 |

Fig. 10. Simulations (c) calculated as for fig. 4 except that now the effects of the contamination layer and of the ion-beam-damaged parts of the specimen are included by subtracting an intensity of 0.3 from the beam that is scattered through angles less than the radius of the centre-stop aperture (the resultant elastic and inelastic image is shown in (a)). The intensity of 0.3 (inferred from fig. 7) is now taken to contribute a hollow cone image as shown in (b), half (as is inferred from fig. 9) of this contribution being simulated as due to elastic scattering and half as would result from inelastic scattering. For (a) $I_{white} = 1$ and $I_{max} = 1.32$, for (b) $I_{white} = 1$ and $I_{max} = 0.78$ and for (c) $I_{white} = 1.5$ and $I_{max} = 1.45$.

the effect of the contamination layer scattering electrons elastically and inelastically past the centre-stop aperture at low specimen thicknesses. Now the contribution to the image from intensity scattered around the centre-stop (fig. 10b) (which is at low thicknesses mainly from the contamination layer and at higher thicknesses from both the contamination layer and plasmon scattering) is, at all thicknesses, of intensity comparable to that which reaches the image only by being scattered by the crystal (fig. 10a): the high resolution detail from these contributions is now of low contrast and is also dominated by the 111 and 002 spacings. The result, when fig. 10a and fig. 10b are added (fig. 10c) to give a first-order approximation of the images now to be expected, is that the

differences in intensity between the layers have been reduced to almost zero with a general reduction in the contrast of the half-spacing fringes, so that fig. 10 is not unlike fig. 6b in general appearance. It should also be noted (comparing these simulations with those in fig. 4) that for the low thicknesses in particular it is, at least for the centre-stop images, the contribution to the *detail* due to the scattering from the contamination which dominates the image. Thus, whilst it has been previously shown that contamination and ion damage can increase the noise in a conventional image [21], we find that it can also cause significant changes in the intensity and high resolution detail in the image.

7. Conclusions

We have shown that the intensity of centre-stop images is much higher than would be expected if only elastic scattering were occurring and if there were no surface contamination. The extra intensity arises from electrons being scattered through angles large enough to pass around the centre-stop aperture, thus adding a "hollow cone" contribution. At low specimen thicknesses most of this scattering is due to elastic and inelastic scattering caused by the contamination layer whilst at greater thicknesses plasmon scattering by the specimen itself becomes the dominant mechanism. Given that these contributions are dominant in centre-stop images they must also be present in conventional bright field high resolution images giving not just a uniform intensity addition but also a contribution to the high resolution detail. Although the addition of a constant background can be ignored by considering only the *pattern* and not the *intensity* or the *contrast* of the image as is normally done when matching conventional high resolution images to conventional simulations, we have shown that both carbon contamination and inelastic scattering modify the *pattern* of centre-stop dark field images and will thus do the same, even if to a lesser extent, for conventional high resolution images.

Acknowledgements

References

[1] E.G. Britton, K.B. Alexander, W.M. Stobbs, M.J. Kelly and T.M. Kerr, GEC J. Res. 5 (1987) 31.
[2] W.M. Stobbs, in: Proc. 3rd Intern. Conf. on Modulated Semiconductor Structures (MSS-III), Montpellier, 1987 [J. Physique 48 (1987) C5-33].
[3] P.M. Petroff, J. Vacuum Sci. Technol. 17 (1980) 1128.
[4] E.G. Britton, PhD Thesis, University of Cambridge (1987).
[5] C.B. Boothroyd, E.G. Britton, F.M. Ross, C.S. Baxter, K.B. Alexander and W.M. Stobbs, in: Microscopy of Semiconditing Materials 1987, Inst. Phys. Conf. Ser. 87, Eds. A.G. Cullis and P.D. Augustus (Inst. Phys. London–Bristol, 1987) p. 15.
[6] H. Kakibayashi and F. Nagata, in: Electron Microscopy 1986, Kyoto, 1986, Eds. T. Imura, S. Maruse and T. Suzuki (Japanese Soc. for Electron Microscopy, Tokyo, 1986) p. 1495.
[7] H. Kakibayashi and F. Nagata, Japan. J. Appl. Phys. 25 (1986) 1644.
[8] D.J. Eaglesham, C.J.D. Hetherington and C.J. Humphreys, in: Mater. Res. Soc. Symp. Proc. 77 (Mater. Res. Soc., Pittsburgh, PA, 1987) p. 473.
[9] E.G. Bithell and W.M. Stobbs, Phil. Mag. A60 (1989) 39.
[10] F.M. Ross, E.G. Britton and W.M. Stobbs, in: EMAG '87, Ed. G.W. Lorimer (Institute of Metals, London, 1988) p. 205.
[11] C.B. Boothroyd, E.G. Britton, F.M. Ross, C.S. Baxter, K.B. Alexander and W.M. Stobbs, in: Microscopy of Semiconducting Materials 1987, Inst. Phys. Conf. Ser. 87, Eds. A.G. Cullis and P.D. Augustus (Inst. Phys. London–Bristol, 1987) p. 195.
[12] Y. Suzuki and H. Okamoto, J. Appl. Phys. 58 (1985) 3456.
[13] C.J.D. Hetherington, J.C. Barry, J.M. Bi, C.J. Humphreys, J. Grange and C. Wood, in: Layered Structures, Epitaxy and Interfaces, 1984, Mater. Res. Soc. Symp. Proc. 37 (Mater. Res. Soc., Pittsburgh. PA, 1985) p. 41.
[14] W.O. Saxton, K.M. Knowles and W.M. Stobbs, in: Electron Microscopy and Analysis 1985, Inst. Phys. Conf. Ser. 78, Ed. G.J. Tatlock (Inst. Phys. London–Bristol, 1985) p. 75.
[15] C.B. Boothroyd and W.M. Stobbs, Ultramicroscopy 26 (1988) 361.
[16] W.M. Stobbs and F.M. Ross in: 1989 NATO Conf. Ser. Bristol, 1988, in press.

[17] W.M. Stobbs and W.O. Saxton, J. Microscopy 151 (1988) 171.

[18] M.J. Hÿtch and W.M. Stobbs, in: EUREM 1988, Inst. Phys. Conf. Ser. 93, Eds. P.J. Goodhew and H.G. Dickinson (Inst. Phys., London–Bristol, 1988) p. 347.

[19] A. Howie, Proc. Roy. Soc. (London) A271 (1963) 268.

[20] R.W. Glaisher, A.E.C. Spargo and D.J. Smith, Ultramicroscopy 27 (1989) 19.

[21] J.M. Gibson and M.L. McDonald, in: Characterization of Defects in Materials, Mater. Res. Soc. Symp. Proc. 82, Eds. R.W. Siegel, J.R. Weertman and R. Sinclair (Mater. Res. Soc., Pittsburgh, PA, 1987) p. 109.

[22] A.J. Bourdillon, W.M. Stobbs, K. Page, R. Home, C. Wilson, B. Ambrose, L.J. Turner and G.P. Tebby, in: EMAG 1985, Inst. Phys. Conf. Ser. 78, Ed. G.J. Tatlock (Inst. Phys., London–Bristol, 1986) p. 161.

[23] R.F. Egerton, Electron Energy Loss Spectroscopy in the Electron Microscope (Plenum, New York, 1986).